Enhancement of the hygroscopic and acoustic properties of indoor plasters with a Super Adsorbent Calcium Alginate BioPolymer

(Article begins on next page)

17 May 2024

Enhancement of the hygroscopic and acoustic properties of indoor plasters with a Super Adsorbent Calcium Alginate BioPolymer

Vincenzo Gentile [a], Michele Libralato [b], Stefano Fantucci [a,*], Louena Shtrepi [a], Giorgia Autretto [a]

[a] *Department of Energy, Politecnico di Torino, C.so Duca degli Abruzzi 24, Turin, Italy*
[b] *Polytechnic Department of Engineering and Architecture, University of Udine, via delle Scienze, 206, Udine, Italy*

A B S T R A C T

The present study introduces a novel-composition lime plaster that contains a Super Adsorbent BioPolymer (SABP) based on Calcium Alginate (CaAlg) for indoor applications, to improve hygrothermal and acoustic comfort. The sorption isotherm of the plaster, the moisture buffering value (MBV), the acoustic absorption, and the thermal conductivity have been assessed. The hygrothermal and acoustic properties of the modified plaster have been compared with those of the original composition to evaluate its performance under different concentrations of CaAlg (between 10 and 30% wt). Adding the CaAlg SABP to a conventional lime plaster consistently enhanced its hygroscopic properties. The results show a substantial increase in the equilibrium moisture uptake (between 10 and 23 fold) and MBV, from 0.9 to 9.3 g/(m²·%RH). The sound absorption coefficient improved by 0.1–0.2 at higher frequencies than 500 Hz. This paper provides detailed information on the characterization of the material. It includes details about using a dynamic vapor sorption (DVS) analyzer to evaluate the sorption isotherm and MBV. It also contains information on the impedance tube method used to measure the acoustic absorption of the material.

1. Introduction

The potential of a material to buffer indoor moisture variations is a property that researchers have investigated to passively improve the comfort of occupants and the safe storage of artifacts [1,2]. This property helps to regulate the indoor humidity of buildings and can help to reduce the mechanical ventilation, and dehumidification loads [3]. Variations in the buffering moisture content can help to maintain the indoor air quality of a building and mitigate mold growth when mechanical ventilation is unavailable.

The Moisture Buffering Value (MBV), measured using NORDTEST, is generally considered to quantify the hygroscopic potential of building materials [4]. Typical building materials, such as gypsum, lime, and wood, have moderate MBV values, ranging from 0.6 to 1.5 g/(m² %RH) [4–6]. However, these values may not be adequate to passively regulate indoor humidity levels, effectively reduce mechanical ventilation and dehumidification, or prevent mold growth. As indoor opaque surfaces are the most common surfaces in buildings, improving the MBV of new plaster materials from low or moderate to high categories, that is, good or excellent [4], could significantly increase the moisture buffering capacity of a building.

1.1. State of the art

A possible methodology to increase the MBV is to produce a composite mortar by blending traditional construction materials, such as lime or cement, with natural or bio-based aggregates, such as wood, in different forms and with other biomasses [7–9]. Many recent works focused on using biopolymers in building materials with different intentions. The utilization of the additives could be focused on reducing the carbon footprint of the materials [10–12] or enhancing the properties [13], including self-healing [14]. Nonetheless, including alternative elements in the mixture can lead to a deterioration of the mechanical properties of the resulting material, particularly when large aggregates are incorporated into the plaster [15].

Substituting large aggregates with natural fibers, such as paper [9,16,17], hemp [18–20], date palm [21–24], straw fibers [25,26], and fiberwood [27], can mitigate the decline in mechanical properties and enhance the MBV. Gradually increasing the fiber content leads to increased MBV, with an average value of approximately 2.5 g/(m^2 %RH) and a reduction in thermal conductivity. Furthermore, in addition to the thermal and mechanical properties, the acoustic properties of such materials have been investigated in several studies. An overview of these works and results is provided in Dahal et al. [28].

Another approach involves combining sorbents, such as zeolites, a metal-organic framework (MOF), and superabsorbent polymers (SAP), with mortar to enhance the final composite moisture level. Despite the high moisture affinity of zeolites, when mixed with sepiolite and perlite-based mortar, they have only demonstrated a 6% increase in the MBV value [29]. A different approach involves covering plasters with a layer of an effective sorbent, such as MOF [30,31], to control the indoor relative humidity. The MBV values of pristine MOF are outstanding (7.4–20.5 g/(m^2 %RH)), and its application as a coating can limit its effective use to that of a thicker layer of material while adding it to the mortar mixture can drastically reduce its effectiveness. On the other hand, using LiCl salt as an additive in a mortar mixture can increase the bulk MBV values by up to 4–10 g/(m^2 %RH) [32].

The presence of SAP particles in a mortar mixture increases its water absorption capacity due to their ionic nature and interconnected chain structure, affecting the workability of the mortar. Consequently, increasing the water-to-binder ratio to maintain plaster workability negatively affects its flexural strength [33]. When SAP concentration is low (less than 0.5% wt), the MBV increase is modest. The average result is around 1.3 g/(m^2 %RH) [34–37]. At higher SAP concentrations (1.5–5% wt), the MBV increase is much more relevant, to 2.5–2.9 g/(m^2 %RH). More than a 100% increase if compared to reference samples. However, the compressive strength has been shown to reduce by 62% for the highest SAP concentrations. Also, thermal conductivity has been reduced from 0.6 to 0.4 W/mK for 1.5% wt [38–40].

Within the SAP family, alginate-derived polymers are increasingly being studied as building material additives due to their effect on the mechanical properties of materials. However, the impact of these polymers on the moisture affinity properties when mixed with plasters still needs to be explored. Murugappan et al. [41] conducted a literature review on the use of alginates in concretes and reported that some alginate-based polymers had an opposite effect on the reduction of the compressive and flexural strength, likely due to their capacity to self-cure concrete [42]. According to a study by Mignon et al. [43], Calcium Alginate (CaAlg) has a more negligible impact on the reduction of compressive strength than other SAP, with a decrease of only 15% from the reference value. However, that study did not explore the effect of CaAlg on the water uptake or the MBV value.

1.2. Objectives

This research has aimed to evaluate how various concentrations of biopolymer aggregates, based on CaAlg, affect the ability of conventional lime plaster to absorb water vapor, its moisture buffering properties, and its thermal conductivity. Additionally, since the inclusion of different aggregates can influence the fundamental properties of the plaster (i.e., flow resistivity, porosity, pore shape factor, and tortuosity, which all affect the sound absorption performance [28,44–47]), an acoustic testing campaign has been conducted to assess their influence on sound absorption.

The following sections illustrate the preparation process of the biopolymer aggregates and the modified plaster, each experimental
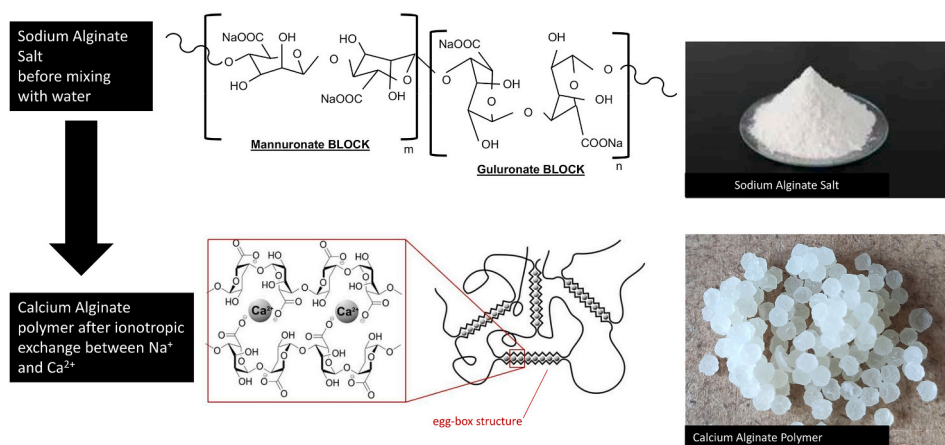

Fig. 1. Schematic representation of the crosslinking process of Sodium Alginate with the substation of monovalent cations Na$^+$ with the divalent Ca^{2+} coming from the CaCl$_2$/water solution. The picture of the resulting Calcium Alginate beads used as hygroscopic aggregate for the composite lime plaster is on the bottom right.

activity, and the final individual results.

2. Methodology

2.1. Materials

2.1.1. Synthesis of calcium alginate SABP

The hygroscopic polymer used in this research is CaAlg, a bio-polymer obtained through the ionotropic gelation [48] of sodium alginate monomers with calcium ions dissolved in a $CaCl_2$/water solution. Sodium alginate (NaAlg) is a salt obtained from the polysaccharide compounds that make up the cell walls of brown algae [49].

The reaction between the different monomers of NaAlg salt (composed of blocks of Mannuronate and Guluronate containing the Na^+ cation) is known as ionotropic gelation. This reaction involves crosslinking parallel monomers through a structure called the "egg box" using a divalent cation. In our case, the divalent cation is Ca^{2+}, obtained by dissolving $CaCl_2$ in demineralized water. Dripping the NaAlg/water gel into the $CaCl_2$/water solution, ionotropic gelation occurs once the interfaces of the two substances are in contact, causing a substitution between Na^+ and Ca^{2+}. The remaining Cl^{2-} in the water solution forms a solvated structure with the Na^+ expelled by the NaAlg monomers [48,50–52]. Fig. 1 depicts the resulting polymer beads, later mixed with mortar powder. The same picture also illustrates the initial sodium alginate's molecular structure and the crosslinked polymer's structure design after the substitution between Na^+ and Ca^{2+} has occurred.

The CaAlg used in this experiment was produced by mixing 1 kg of deionized water with 20 g of a gelling agent, sodium salt from alginic acid, and rapidly stirring the mixture at a high rotational speed until reaching the complete solution homogeneity. The gel was degassed under vacuum at an absolute pressure of 200–500 mbar and dripped into a crosslinking salt solution, prepared by mixing 1 L of deionized water with 133 g of dehydrated $CaCl_2$. The bath was left to rest for approximately 12 h to complete the diffusion of the Ca^{2+} cations and the subsequent crosslinking of the beads. Finally, the crosslinked beads were drained and thoroughly rinsed with demineralized water to remove any excess salt and were then dried in a ventilated oven at 70°C.

2.1.2. Reference mortar

The used mortar was a cement-free commercial product based on a mix of natural hydraulic lime (2.5–5%), crystalline silicon (0.5–1% with a diameter <1 μm), recycled material (~23%), and fillers (70–75%) based on limestone, pozzolana and polypropylene microfibers (diameter ~10 μm). Detailed SEM images of the reference mortar are reported in the supplementary information S6. Further, the manufacturer reports the following performance information: the maximum dimension of aggregates 2.5 mm (EN1015-1), the apparent volumetric mass of 1500 kg/m³, and a porosity of the fresh plaster higher than 20% (EN 1015-7). When the mortar powder is pasted with 15% water, the workability time is 60 min (EN1015-9), and the compressive strength after 28 days is 3.5–7.5 N/mm². Water absorption due to capillarity is 3.5 kg/m² according to EN 1015-18 for a renovation plaster. The resistance factor of water vapor diffusion equals 10 according to EN 1015-19.

2.1.3. Samples preparation

CaAlg beads with a diameter of 2–3 mm (Fig. 2a, 2b) were first homogeneously mixed with the mortar powder and then mixed with water (Fig. 2c). Eight different samples were prepared, two for the reference material (A00) and six samples (two for each composition) with increasing concentrations of CaAlg (B01, B02, and B03). The increase in the CaAlg concentration required a slightly larger amount of water. Indeed, the water ratio was increased from 17% to 22% to maintain the mortar workability level similar to reference
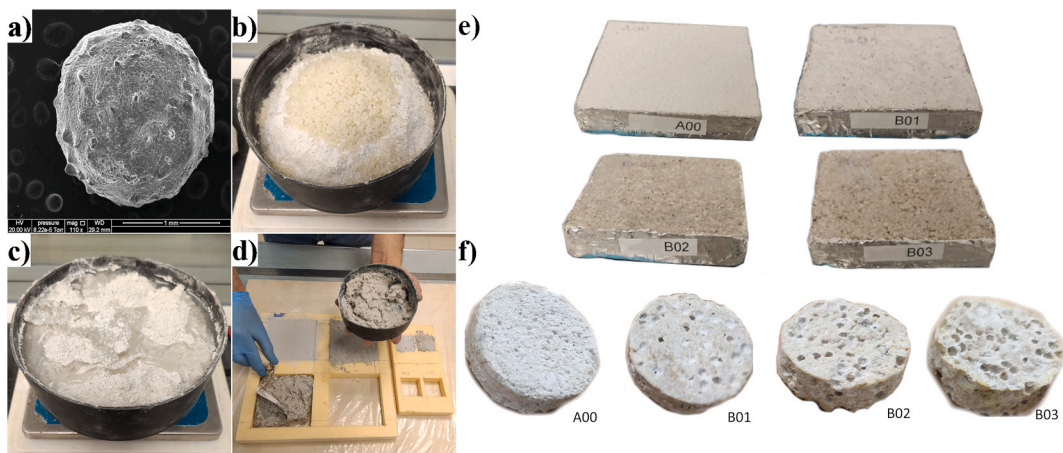

Fig. 2. Pictures of the preparation steps of the composite mortar and the resulting samples. a) magnification of a CaAlg bio-polymer bead obtained using scanning electron microscopy (SEM) - FEI Quanta 200. b) mixing the CaAlg beads with dry mortar powder in a concentration, as reported in Table 1 for the CaAlg/mortar parameter. c) mixing water with the mortar powder and CaAlg beads in the proportions indicated in Table 1 for the water/binder ratio. d) pouring the wet composite mortar into two different square molds. e) composite mortar samples taken from the more extensive square molds after one week of drying at ambient T and RH. f) circular samples after manipulating the smaller square samples after one week of drying at ambient T and RH.

A00. The evaluation of the workability level was only qualitative. The different mixtures were poured into two different-sized square molds (Fig. 2d) and left to rest at ambient temperature and humidity for about one week to complete the drying process. To determine the dry mass (m_{dry}) of each sample, they were dried in a ventilated oven at 70°C for 72 h and weighed on scales (reproducibility of 0.1 g) to determine the dry mass (m_{dry}) of each sample.

The final values and other information, such as the sample dimensions and CaAlg concentrations, are listed in Table 1. Smaller cylindrical samples were subsequently cut and sanded to fit into the Dynamic Vapor Sorption (DVS) device and the impedance tube for acoustic tests. Furthermore, the B03 sample was deliberately cracked open to evaluating beads distribution within the internal volume. It was observed under an FEI Quanta 200 scanning electron microscope (SEM), as reported in Fig. 3. Moreover, a reference sample was also analyzed, and its results can be found in the supplementary information (S6) section.

The SEM images demonstrate that the differential retraction between the mortar and CaAlg beads caused spherical empty spaces to form around each polymer particle during the drying process of the composite material, as depicted in the SEM magnifications in Fig. 3. The number and the density of these holes increased as the concentration of CaAlg increased, as clearly shown in Fig. 2f. The beads appear covered with loose mortar from the cavity formed during drying. In the case of the B03 sample, the cavity had a size of around 2.5 mm, while the inner particle itself was about 1.5 mm. Moreover, interconnected cavities readily form throughout the internal volume as the concentration of aggregates increases.

2.2. Isotherms

The moisture sorption isotherms of the four compositions were determined at the Thermal Systems Lab (DPIA University of Udine) using a Vsorp Basic DVS analyzer (ProUmid) on cylindrical samples. The equilibrium conditions were measured at 0%, 40%, 50%, 60%, and 70% RH for adsorption and desorption to obtain the isotherms at a precision of ±0.1% RH and constant temperature of 23 ± 0.1°C. The equilibrium points were limited to below 70% RH because the B02 and B03 samples had shown the formation of liquid drops on the sample surfaces in a preliminary measurement at 80% RH. This deliquescent behavior has not been investigated in this work. The pieces were kept in a controlled environment with an air velocity of 0.15 m/s and were automatically weighed on scales every 30 min. The scales had a reproducibility of 0.1 mg. The moisture content (u) of each sample was calculated as follows:

$$u = \frac{m - m_{dry}}{m_{dry}} \left[\frac{g_{H_2O}}{g_{dry\,mass}} \right] \tag{1}$$

where m is the mass of the sample in g and m_{dry} is the mass of the dry sample in g. The equilibrium condition is defined as a limit of the variation in mass over time. In particular, mass variations lower than 0.001% for more than 300 min is the determining criterion to establish the equilibrium condition. This criterion follows the equilibrium condition defined in the ISO 12571:2021 standard, albeit using a shorter period as the reference. ISO 12571:2021 defines an equilibrium condition if, after three weighings made 24 h apart, the change in mass is lower than 0.1% of the total mass. The samples were dried in the DVS at 0% + 0.1 RH (-40°C dew point) and at 23°C before the adsorption test.

2.3. Moisture buffering tests

The moisture buffering performance of the various developed mortars was measured, through the MBV test, using two different instruments:

- a climatic chamber
- the DVS device

Both procedures complied with the temperature and relative humidity condition cycles of the NORDTEST protocol [4]. In both tests, the temperature was constant at 23°C, while the RH varied as a 24-h square wave with 75% for 8 h and 33% for the residual 16 h. In both cases, since it was not known if the tested samples had a thickness that exceeded the moisture penetration depth of the given material, it was evaluated the practical moisture buffer value ($MBV_{practical}$) [4].

Table 1

Data specifications of the different compositions of the A00, B01, B02, and B03 samples. The table reports the mass percentage ratio of mortar/water/CaAlg, bulk densities, gross geometries, and dry masses of the samples used for the different experimental tests.

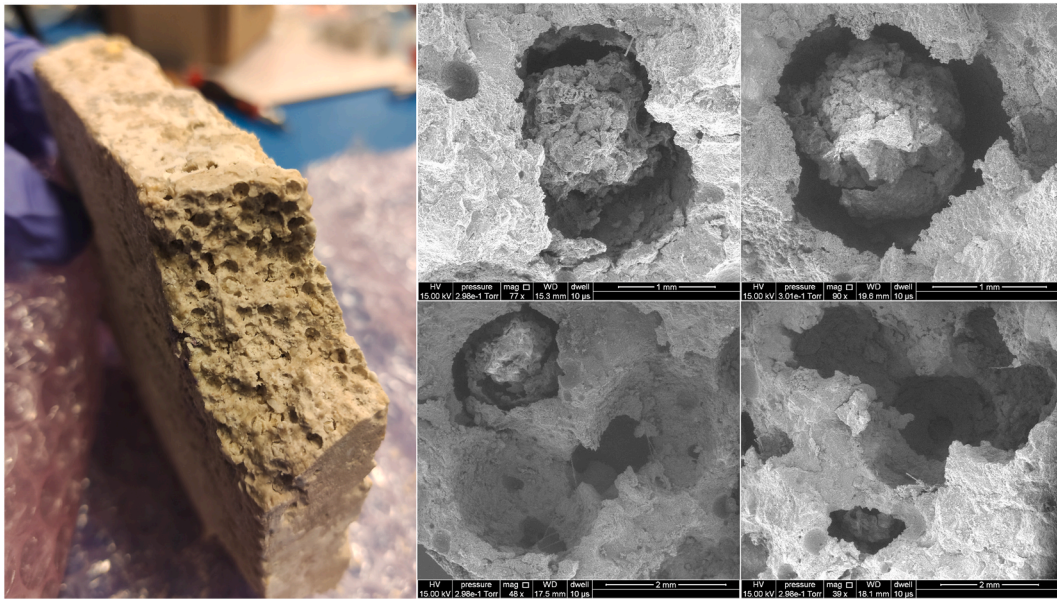|		A00	B01	B02	B03
Mortar mass	[g]	500	500	450	400
Water/binder ratio	[%]	17	17	21	22
CaAlg/mortar ratio	[%]	0	10	20	30
Density (dry)	[kg/m^3]	1761	1783	1611	1566
Square Sample - Dry mass (m_0)	[g]	437.5	482	439	420.5
Thickness	[mm]	20.8	22.4	22.1	22.4
Sizes	[mm]	109.4	109.1	110.8	109.5
		109.3	112.1	111.1	109.7
Circular Sample - Dry weight (m_0)	[g]	18.6	21.5	17.5	14.5
Thickness	[mm]	13.9	14.1	13.6	13.5
Diameter	[mm]	34.5	34.5	34.5	34.5

Fig. 3. Different SEM magnifications of the cracked B03 sample.

2.3.1. The MBV test in the climatic chamber

To perform the test, all the bottom and sides of the square prismatic samples (A00, B01, B02, B03) were sealed with a first layer of acrylic silicon and a final layer of aluminum tape. This procedure left only the upper surface exposed to air and moisture [4].

The four samples were first preconditioned in an ATT DM340 climatic chamber at 23 ± 0.3°C and 50 ± 3%RH until the mass stabilization, and then 75%RH (8h) and 33%RH (16h) cycles were repeated five times each. However, as shown in Fig. 4, only the last three consecutive cycles were chosen for the MBV calculation due to a 2% deviation of the average RH from the prescribed set point. Table 2 shows the average temperature and relative humidity conditions during the tests and the average difference in the relative humidity between the adsorption and desorption cycles.

2.3.2. The MBV test in the DVS device

The MBV was also evaluated in the DVS device at the Thermal Systems Lab (DPIA University of Udine). Because of the size limitations of the device, the test was conducted following the procedure presented in Rode et al. [4], except for the size of the exposed surface of each sample, which was smaller than the recommended value of 0.01 m². The samples were placed in the device trays with the free surface facing upward. The samples were first dried to 0% RH (dew point temperature at -40°C) at 23 °C and later conditioned to 50% RH at the same temperature. The samples were then subjected to cycles, as in 2.3.1, and weighed automatically every 30 min.
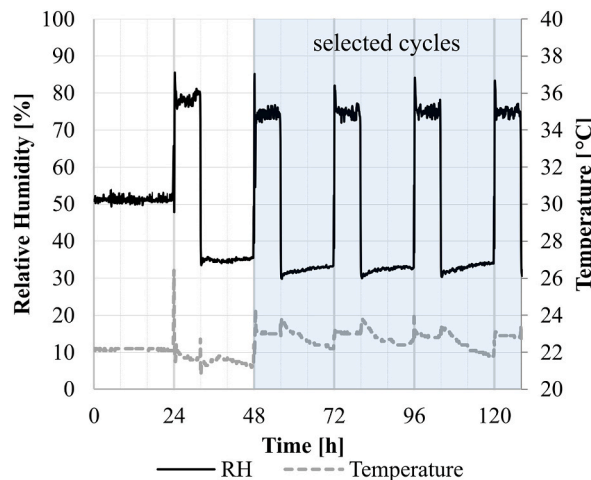

Fig. 4. The graph shows the temperature and relative humidity conditions measured during the MBV test with the climatic chamber.

Table 2
Test conditions. Average temperature T_{avg}, relative humidity RH_{avg}, and variation in the relative humidity between the adsorption, $\Delta RH_{abs.}$, and desorption, $\Delta RH_{des.}$, cycles.

cycle	RH_{avg} [%]	T_{avg} [°C]	ΔRH_{des} [%]	$\Delta RH_{abs.}$ [%]	Selected values
1	78.2	21.8			
	35.0	21.5	43.2		no
2	74.0	23.1		39.0	no
	32.3	22.8	41.6		yes
3	75.0	23.1		42.6	yes
	32.4	22.8	42.6		yes
4	75.3	22.9		42.9	yes
	33.0	22.4	42.2		yes
5	75.1	22.9		42.1	yes
	39.9	22.9	35.2		no

2.4. Acoustic properties

The acoustic measurements were performed on the four typologies (A00, B01, B02, and B03) in an ISO 10534-2 impedance tube [53] (two-microphone technique) to assess the normal-incidence sound absorption coefficient. The advantage of this method is that it offers the possibility of obtaining measurements using small samples, which are appropriate for the aim of this investigation. An HW-ACT-TUBE impedance tube (picture in S7 of the supplementary information) at the Applied Acoustics Laboratory (Department of Energy, Politecnico di Torino) was used for these measurements. This device has an internal diameter of 35 mm and is equipped with two ¼'' flush-mounted GRAS 46BD. The method allowed accurate sound pressure amplitude and phase measurements over the whole frequency range of interest, i.e., 100–5000 Hz [53]. A white noise source, i.e., a 2'' aluminum driver, produces continuous high sound levels (100 dB) inside the tube, thus ensuring a high signal-to-noise ratio by design, and it generates a flat spectrum over the 100–5000 Hz frequency range.

The normal-incidence absorption coefficient (α_0) was measured for each composition, considering the effect on both sides of the sample: front and back (the different superficial characteristics of the two sides are depicted in Fig. 5). The aim was to investigate the effects of any superficial differences due to the casting conditions. Moreover, the edges of the samples had been adequately sealed with a thin Teflon tape to even out the irregularities generated by the cutting technique and to fill the gaps (<1 mm) between the sample and tube [54].

2.5. Thermal conductivity

The equivalent thermal conductivity (λ_{eq}) was measured, at the HigroThermal Characterization Lab (Department of Energy, Politecnico di Torino), according to the EN 12664:2002 standard [55]. An HFM FOX600 (Heat Flow Meter) instrument (Fig. 6a) was used to conduct the test. Since the sample was smaller than the measuring area of the HFM (~254 × 254 mm), a neoprene frame (390x390 × 20 mm) was used to hold the samples in place (Fig. 6b). The neoprene frame was tested at an average temperature of 23°C ($T_{upper\ plate}$ = 18°C; $T_{lower\ plate}$ = 28°C; ΔT = 10°C), and a thermal conductivity of 0.035 W/mK was obtained.

The assembled sample (mortar within the neoprene frame) was placed inside the instrument, positioned centrally over the two plates, and tested under the same conditions as the neoprene frame. Moreover, the test was conducted under dry conditions and after preconditioning the sample in a ventilated oven at 60°C until reaching a constant mass [56]. The thermal conductivity was then measured at an ambient condition ($\lambda_{23,\ dry}$) of 23 °C.

Fig. 5. The A00, B01, B02, and B03 samples inside the Impedance tube. a) front and b) back of each sample.
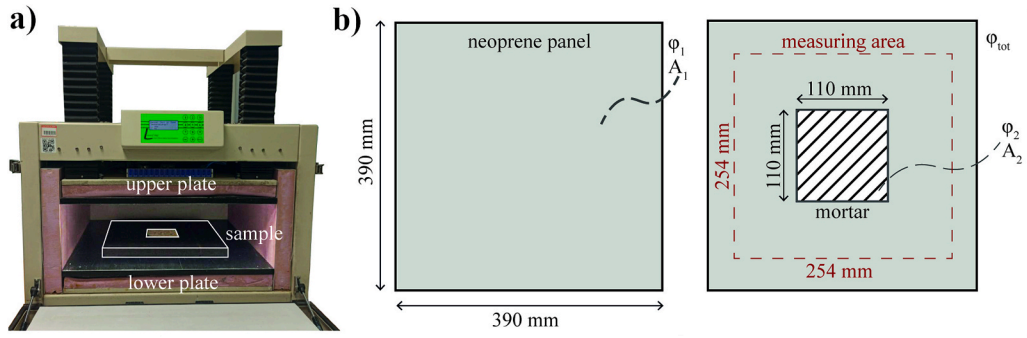
Fig. 6. a) A sample inside the DHFM apparatus; b) Neoprene panel and mortar placed inside the neoprene frame.

The equivalent thermal conductivity of the different samples was determined by calculating the heat flow through the surface of the mortar (equation (2)):

$$\varphi_2 = \frac{\varphi_{TOT} \times A_1 - \varphi_1 \times (A_1 - A_2)}{A_2} \left[\frac{W}{m^2}\right] \tag{2}$$

where φ_{TOT} is the heat flow through the whole sample (neoprene ring containing the plaster); A_1 is the area of the whole sample; φ_1 is the heat flux across the previously tested neoprene sample itself, and A_2 is the surface area of the plaster tile (Fig. 6b).

Finally, the thermal conductivity of the samples was calculated according to equation (3):

$$\lambda = \frac{\varphi_2}{\Delta T} \times t \left[\frac{W}{mK}\right] \tag{3}$$

where ΔT is the temperature difference between the two plates of the Heat Flux Meter apparatus and t is the thickness of the sample.

3. Results and discussion

After the CaAlg beads are removed from the reticulation bath of $CaCl_2$/water and thoroughly rinsed with demineralized water, some residual deposits of CaCl2 and NaCl may still exist on the polymer surface. Even though these residues are minimal, they can contaminate the final composite plaster with chlorides. Such contamination can have negative implications for the long-term durability of the plaster, as documented in the literature [57–59]. The presence of chlorides, such as NaCl, CaCl2, and MgCl2, is known to initiate or accelerate the corrosion of reinforcement steel, cause freeze-thaw damage, and result in white efflorescence. However, it should be noted that the minimal contamination introduced through this methodology may also positively impact the mortar's compressive and flexural strength during the early stages [60].

Including CaAlg beads in the mortar mix required an additional but marginal amount of water proportional to the aggregates concentration. This procedure was to obtain qualitative homogenous workability among the different samples. Therefore, the water ratio increased from 17% (reference sample) to 21% (highest CaAlg concentration).
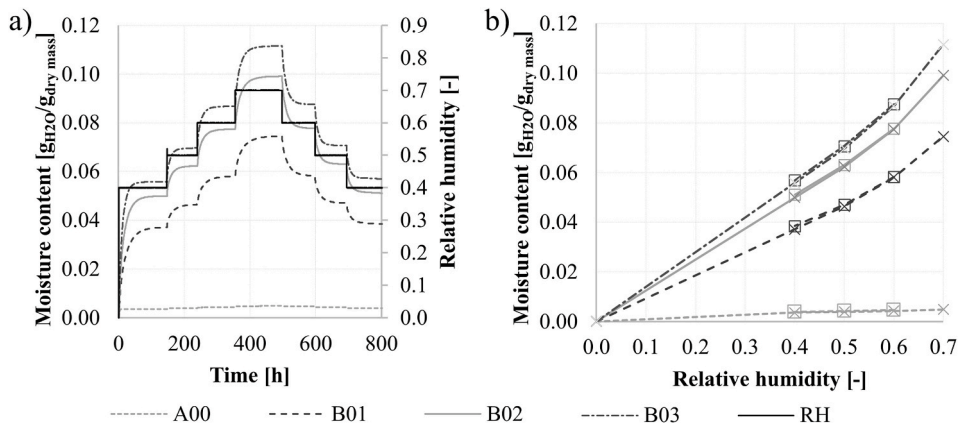

Fig. 7. On the left: Dynamic measurement of the moisture adsorbed by the samples in the DVS analyzer. On the right: Adsorption and desorption isotherms measured using the DVS analyzer. Crosses represent the adsorption curve points, while squares represent the desorption points, and they practically overlap and show a negligible hysteresis effect.

Simultaneously, the hardening process caused the CaAlg beads to contract, forming air gaps within the samples, as visible from SEM images. The polymer beads absorbed the water when added during the mixing phase. The difference between the swelled volume and the contracted one resulted from the hardening stage led to the formation of air gaps. The higher presence of CaAlg likely induces the formation of interconnected air gaps.

In the end, the proportional increase in the polymer concentration reduces sample density, as shown in Table 1.

The mechanical properties of the hardened plaster were likely affected by the increased water content and decreased density. However, no visible signs of stiffness degradation were observed in any of the different compositions. The used reference mortar belongs to the CSII category as per EN 998-1. Future research should concentrate on verifying this category. The only noticeable change was in the surface appearance, where spherical aggregates were observed, particularly in the B03 sample.

3.1. Sorption isotherms

The changes in the sample weights are shown in Fig. 7a as the relative humidity conditions increase and decrease over time. The composites responded well to both increases and decrease in humidity, with noticeable differences between the two phases (sorption and desorption), relative to the time it took to reach equilibrium (see S2 and S3 in the supplementary information). However, although it took more than 100 h to achieve each equilibrium point, in most cases, the mass variation of the samples reached 95% of the equilibrium value in less than 50% of the total required time.

CaAlg influenced the water vapor uptake to a great extent and confirmed a proportionality between its concentration and the variations of the mass under equilibrium. Fig. 7b shows the adsorption and desorption equilibrium points at 23°C. Table S1 of the supplementary information reports in detail the values of each equilibrium point. The curves show minor and mostly overlapping differences, with a maximum absolute difference of 0.14% (g_{H_2O}/g_{dry}) of discrepancy at 40%RH for the B01 sample. The standard deviation of the last ten measurements before reaching the equilibrium conditions was consistently below 0.004% (g_{H_2O}/g_{dry}) for each sample and testing condition.

3.2. MBV test

Fig. 8 presents the results of both MBV tests, while Table 3 recalls all the differences between the two test procedures (climatic chamber versus DVS). The final MBV tests in the climatic chamber were restricted to three cycles because of a 3% deviation of the RH from the prescribed values during the 1st and 5th cycles. A comparison of the average result, weighted over three cycles (MBV_3) instead of 5 (MBV_5), led to minimal differences in the final results, as shown in Table 3.

Furthermore, the differences in thickness and surface manipulation were responsible for some differences in the related results. When the moisture penetration depth in the material was less than the thickness of the sample, the measured MBV was unaffected. When the thickness of the sample was less than the penetration depth, the thinner samples were expected to reach saturation earlier and uptake a smaller absolute quantity of moisture.

Moreover, the surface treatment used on the samples in the DVS analyzer test led to the loss of some alginate beads. This, combined with the inhomogeneity of samples, resulted in a modified CaAlg concentration. Consequently, the smaller sample has shown a reduced equilibrium moisture content and MBV value. This effect became more relevant as more CaAlg particles were dispersed within the plaster. From a comparison of the results, it can be seen that the most significant difference was for the B03 samples, while minimal differences were observed for the other samples.

The improvement achieved in this research refers to a greater MBV increase, with respect to the reference material, and a higher MBV value than in the other experiments in literature in which mortar composites were used with other polymers or sorbents [24–35]. To the best of the authors' knowledge, the only research that has shown comparable results is that of Yang et al. [32], who produced a sample with a similar thickness by adding lithium chloride to a conventional mortar (1–8% wt) and obtained practical MBV values within the 4–10.5 g/(m^2 %RH) range.

3.3. Acoustic properties

The measurement results are presented in Fig. 9 for each material typology, considering the effect on both sides of the sample. The
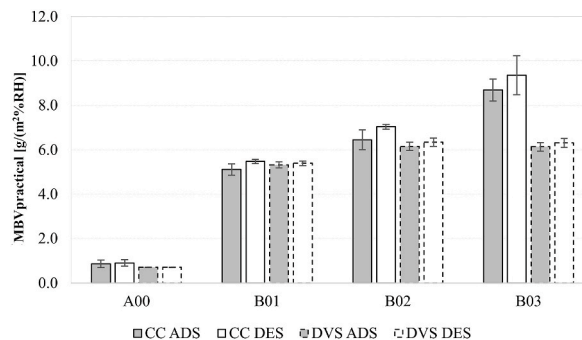

Fig. 8. The MBV values (one for adsorption and one for desorption) as measured in the two tests with the different experimental setups. The whiskers indicate the standard deviation.

Table 3
Differences between the MBV test procedures.

		Climatic chamber	DVS analyzer
Exposed surface		$\sim$0.00121 m^2	$\sim$0.0009 m^2
Sample thickness		$\sim$21 mm	13 mm
Weighing method		Manual	Automatic
Surface treatment		None	Sanded
A00	**MBV$_3$**	0.88	–
	MBV$_5$	0.90	0.7
B01	**MBV$_3$**	5.29	–
	MBV$_5$	5.47	5.35
B02	**MBV$_3$**	6.74	–
	MBV$_5$	7.03	6.24
B03	**MBV$_3$**	9.02	–
	MBV$_5$	9.36	6.22

frequency-dependent sound absorption was evaluated and is presented in third-octave bands. It can be observed that there are only some slight differences ($<$0.10) between the two sides of the sample for each typology, except for sample B03, which presents significant differences above 315 Hz. These differences are presumably associated with the variations of the superficial porosity since some of the alginate beads might have been lost while moving the samples from the casting during the different measurement stages.

The best performance was achieved for the B03_back sample. However, this sample appears to be compatible with the B02_back sample up to 2000 Hz. Both samples outperformed the A00 sample at lower ($<$800 Hz) and higher ($>$1600 Hz) frequencies. On the other hand, the B03 sample results for the front side show a lower sound absorption, which is compatible with the B01 results. This variability can be considered as a promising outcome. The performance could be further improved by designing the aggregate content with values of up to 0.40 for high frequencies. Moreover, the B03 sample shows a more even distribution of the frequency-dependent sound absorption, which makes it useful for room-acoustic purposes in several applications [61]. This result is presumably connected to the density increase in the interconnected cavities and to variations in the superficial porosity [4,23].

3.4. Thermal conductivity

Table 4 summarises the measured equivalent thermal conductivities and each parameter required for equations (2) and (3) for each sample and concentration.

As for the acoustic measurements, the increase in the macroscopic porosity associated with the CaAlg concentration influenced the thermal conductive properties. Indeed, the thermal conductivity of the samples decreases as the CaAlg concentration increases. B02 and B03 show progressively lower $\lambda_{23,\,dry}$ than B01. This behavior is presumably due to the increase of the air cavities within the plasters and the consequent reduction in the bulk density of the composite from 1783 to 1566 kg/m^3.

On the other hand, although the densities of the A00 and B01 samples are similar, B01 is much more conductive than A01 (0.408 W/mK for A00 and 0.892W/mK for B01). Presumably, the air cavities generated for a CaAlg concentration of 10% do not sufficiently compensate for the increase of specific thermal conductivity driven by the presence of CaAlg.

4. Conclusions

In this study, the effect of including calcium alginate biopolymers in a lime-based plaster was investigated. Test results revealed that:

- Blending calcium alginate biopolymer particles (average diameter $\sim$1.5 mm) with commercial mortar significantly improved hygroscopic properties. Increasing biopolymer concentration (10–30%) correlated with higher moisture uptake and MBV. CaAlg increased water uptake by over 10–23 fold within a 30–70% humidity range.
- With the highest CaAlg concentration, practical MBV is higher than 9. The MBV results and methodology have been validated with two different instruments (a climatic chamber and a dynamic vapor sorption analyzer) and in two different laboratories. The obtained results were coherent for samples A00, B01, and B02. The inhomogeneity and high concentration of CaAlg of composition B03 affected the reproducibility of the data.
- The expansion of CaAlg beads during water mixing leads to the formation of pseudospherical cavities around the aggregates. The count of empty cavities is increasing as *i*) the higher CaAlg concentration, *ii*) the reduced sample density, *iii*) the decreased thermal conductivity, and *iv*) the increase of sound absorption across different frequencies.

Despite the higher water content and lower density may have impacted the mechanical properties of the hardened plaster, no visible signs of stiffness degradation were observed across various compositions. The reference mortar belongs to the CSII category per EN 998-1. The only noticeable change was in the surface appearance, with spherical aggregates notably present in the B03 sample. Future research should focus on verifying this categorization and the influence of different particle volumetric shrinking ratios. Further optimization of the normal-incidence absorption coefficient is possible by redesigning the microstructural configuration of the mix and the distribution of the cavities resulting from the shrinking of CaAlg. Indeed, the tortuosity and flow resistivity could be further increased by adequately controlling the void ratio and aggregate type.
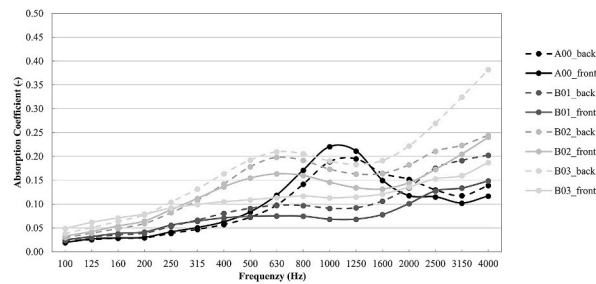
Fig. 9. The normal-incidence sound absorption coefficient of each tested typology.

Table 4
The equivalent thermal conductivity test results, together with the main parameters and testing conditions.

Sample	Thickness	ΔT	A	φ_{tot}	φ_2	$\lambda_{23,\,dry}$
	[mm]	[°C]	[m^2]	[W/m^2]	[W/m^2]	[W/mK]
Neoprene panel	23.7	10	0.152	14.88	–	0.035
A00	23.6	10	0.0123	27.68	172.95	0.408
B01	23.1	10	0.0127	45.77	386.23	0.892
B02	23.7	10	0.0128	35.99	266.41	0.632
B03	23.1	10	0.0128	34.64	250.38	0.579

Author statement

Vincenzo Gentile: Conceptualization, Methodology, Investigation, Data curation, Writing - Original Draft, Writing – Review & Editing, Visualization, Supervision. Michele Libralato: Investigation, Data curation, Writing – Original Draft, Writing – Review & Editing, Visualization. Stefano Fantucci: Conceptualization, Investigation, Writing – Original Draft, Writing – Review & Editing, Supervision. Louena Shtrepi: Investigation, Data curation, Writing – Original Draft, Writing – Review & Editing, Visualization. Giorgia Autretto: Investigation, Writing – Original Draft.

Authors declaration

We wish to confirm that there are no known conflicts of interest associated with this publication and there has been no significant financial support for this work that could have influenced its outcome.

We confirm that the manuscript has been read and approved by all named authors and that there are no other persons who satisfied the criteria for authorship but are not listed. We further confirm that the order of authors listed in the manuscript has been approved by all of us.

We confirm that we have given due consideration to the protection of intellectual property associated with this work and that there are no impediments to publication, including the timing of publication, with respect to intellectual property. In so doing we confirm that we have followed the regulations of our institutions concerning intellectual property.

We understand that the Corresponding Author is the sole contact for the Editorial process (including Editorial Manager and direct communications with the office). He is responsible for communicating with the other authors about progress, submissions of revisions and final approval of proofs. We confirm that we have provided a current, correct email address which is accessible by the Corresponding Author and which has been configured to accept email from: *stefano.fantucci@polito*.it.

Declaration of competing interest

The authors declare that they have no known competing financial interests or personal relationships that could have influenced the work reported in this paper.

Data availability

I have added some of the data as supplementary information. Additional data can be requested

Acknowledgments

for her invaluable assistance in creating the graphical abstract.

Appendix A. Supplementary data

Supplementary data to this article can be found online at https://doi.org/10.1016/j.jobe.2023.107147.

References

[1] V. Cascione, D. Maskell, A. Shea, P. Walker, A review of moisture buffering capacity: from laboratory testing to full-scale measurement, Construct. Build. Mater. 200 (2019) 333–343.
[2] H. Janssen, J.E. Christensen, Hygrothermal optimisation of museum storage spaces, Energy Build. 56 (2013) 169–178.
[3] C.J. Simonson, M. Salonvaara, T. Ojanen, The effect of structures on indoor humidity - possibility to improve comfort and perceived air quality, Indoor Air 12 (2002) 243–251.
[4] C. Rode, et al., Moisture Buffering of Building Materials, Technical University of Denmark, Department of Civil Engineering, 2005.
[5] V. Cascione, D. Maskell, A. Shea, P. Walker, The moisture buffering performance of plasters when exposed to simultaneous sinusoidal temperature and RH variations, J. Build. Eng. 34 (2021), 101890.
[6] A. Ranesi, P. Faria, M.D.R. Veiga, Traditional and modern plasters for built heritage: suitability and contribution for passive relative humidity regulation, Heritage 4 (2021) 2337–2355.
[7] F. Mnasri, S. Bahria, M.E.A. Slimani, O. Lahoucine, M. El Ganaoui, Building incorporated bio-based materials: experimental and numerical study, J. Build. Eng. 28 (2020), 101088.
[8] S. Palmieri, et al., Pilot scale cellulose recovery from sewage sludge and reuse in building and construction material, Waste Manag. 100 (2019) 208–218.
[9] M.L. Vares, A. Ruus, N. Nutt, A. Kubjas, J. Raamets, Determination of paper plaster hygrothermal performance: influence of different types of paper on sorption and moisture buffering, J. Build. Eng. 33 (2021), 101830.
[10] M.M. Santos, et al., Reducing cement consumption in mortars by waste-derived hydrochars, J. Build. Eng. 75 (2023), 106987.
[11] D. Shanmugavel, T. Selvaraj, R. Ramadoss, S. Raneri, Interaction of a viscous biopolymer from cactus extract with cement paste to produce sustainable concrete, Construct. Build. Mater. 257 (2020), 119585.
[12] T.R. da Silva, P.R. de Matos, L.U.D. Tambara Júnior, M.T. Marvila, A.R.G. de Azevedo, A review on the performance of açaí fiber in cementitious composites: characteristics and application challenges, J. Build. Eng. 71 (2023), 106481.
[13] H. Affan, W. Arairo, J. Arayro, Mechanical and thermal characterization of bio-sourced mortars made from agricultural and industrial by-products, Case Stud. Constr. Mater. 18 (2023), e01939.
[14] C. Zhang, et al., Biopolymer recovery from waste activated sludge toward self-healing mortar crack, Sci. Total Environ. 858 (2023), 160107.
[15] R.M. Novais, et al., Multifunctional cork – alkali-activated fly ash composites: a sustainable material to enhance buildings' energy and acoustic performance, Energy Build. 210 (2020), 109739.
[16] C. Giosuè, A. Mobili, G. Toscano, M.L. Ruello, F. Tittarelli, Effect of biomass waste materials as unconventional aggregates in multifunctional mortars for indoor application, Procedia Eng. 161 (2016) 655–659.
[17] N. Nutt, A. Kubjas, L. Nei, Adding waste paper to clay plaster to raise its ability to buffer moisture, Proc. Est. Acad. Sci. 69 (2020) 179–185.
[18] T. Colinart, D. Lelievre, P. Glouannec, Experimental and numerical analysis of the transient hygrothermal behavior of multilayered hemp concrete wall, Energy Build. 112 (2016) 1–11.
[19] B. Mazhoud, F. Collet, S. Prétot, C. Lanos, Effect of hemp content and clay stabilization on hygric and thermal properties of hemp-clay composites, Construct. Build. Mater. 300 (2021), 123878.
[20] Y. Jiang, et al., Improvement of water resistance of hemp woody substrates through deposition of functionalized silica hydrophobic coating, while retaining excellent moisture buffering properties, ACS Sustain. Chem. Eng. 6 (2018) 10151–10161.
[21] Y. Zouaoui, F. Benmahiddine, A. Yahia, R. Belarbi, Hygrothermal and mechanical behaviors of fiber mortar: comparative study between palm and hemp fibers, Energies 14 (2021) 1–16.
[22] Y. Abdellatef, M.A. Khan, A. Khan, M.I. Alam, M. Kavgic, Mechanical, thermal, and moisture buffering properties of novel insulating hemp-lime composite building materials, Materials 13 (2020) 1–18.
[23] N. Chennouf, B. Agoudjil, A. Boudenne, K. Benzarti, F. Bouras, Hygrothermal characterization of a new bio-based construction material: concrete reinforced with date palm fibers, Construct. Build. Mater. 192 (2018) 348–356.
[24] R. Belakroum, et al., Design and properties of a new sustainable construction material based on date palm fibers and lime, Construct. Build. Mater. 184 (2018) 330–343.
[25] A. Antunes, P. Faria, V. Silva, A. Brás, Rice husk-earth based composites: a novel bio-based panel for buildings refurbishment, Construct. Build. Mater. 221 (2019) 99–108.
[26] I. Niang, et al., Hygrothermal performance of various typha–clay composite, J. Build. Phys. 42 (2018) 316–335.
[27] L. Senff, G. Ascensão, V.M. Ferreira, M.P. Seabra, J.A. Labrincha, Development of multifunctional plaster using nano-TiO2 and distinct particle size cellulose fibers, Energy Build. 158 (2018) 721–735.
[28] R.K. Dahal, B. Acharya, A. Dutta, Mechanical, thermal, and acoustic properties of hemp and biocomposite materials: a review, J. Compos. Sci. 6 (2022).
[29] Y. Wu, G. Gong, C.W. Yu, Z. Huang, Proposing ultimate moisture buffering value (UMBV) for characterization of composite porous mortars, Construct. Build. Mater. 82 (2015) 81–88.
[30] M. Qin, P. Hou, Z. Wu, Wang, J. Precise humidity control materials for autonomous regulation of indoor moisture, Build. Environ. 169 (2020), 106581.
[31] K. Zu, M. Qin, C. Rode, M. Libralato, Development of a moisture buffer value model (MBM) for indoor moisture prediction, Appl. Therm. Eng. 171 (2020), 115096.
[32] Z. Yang, W. Zhang, X. Lin, Q. Xiong, Q. Jiang, Optimization of minor-LiCl-modified gypsum as an effective indoor moisture buffering material for sensitive and long-term humidity control, Build. Environ. 229 (2023), 109962.
[33] L. Senff, et al., Development of mortars containing superabsorbent polymer, Construct. Build. Mater. 95 (2015) 575–584.
[34] J. Fořt, J. Šál, J. Žák, Combined effect of superabsorbent polymers and cellulose fibers on functional performance of plasters, Energies 14 (2021).
[35] H. Gonçalves, et al., Development of porogene-containing mortars for levelling the indoor ambient moisture, Ceram. Int. 40 (2014) 15489–15495.
[36] L. Senff, G. Ascensão, D. Hotza, V.M. Ferreira, J.A. Labrincha, Assessment of the single and combined effect of superabsorbent particles and porogenic agents in nanotitania-containing mortars, Energy Build. 127 (2016) 980–990.
[37] J. Vieira, et al., Functionalization of mortars for controlling the indoor ambient of buildings, Energy Build. 70 (2014) 224–236.
[38] J. Fořt, M. Doleželová, V. Kočí, R. Černý, Functional properties of sap-based humidity control plasters, Polymers 13 (2021).
[39] H. Gonçalves, et al., The influence of porogene additives on the properties of mortars used to control the ambient moisture, Energy Build. 74 (2014) 61–68.
[40] J. Fořt, et al., Characterization of responsive plasters for passive moisture and temperature control, Appl. Sci. 10 (2020) 1–16.
[41] V. Murugappan, A. Muthadhi, Studies on the influence of alginate as a natural polymer in mechanical and long-lasting properties of concrete – a review, Mater. Today Proc. 65 (2022) 839–845.

[42] S. Xu, X. Liu, A. Tabaković, E. Schlangen, Investigation of the potential use of calcium alginate capsules for self-healing in porous asphalt concrete, Materials 12 (2019) 1–13.

[43] A. Mignon, et al., Alginate biopolymers: counteracting the impact of superabsorbent polymers on mortar strength, Construct. Build. Mater. 110 (2016) 169–174.

[44] N. Neithalath, J. Weiss, J. Olek, Characterizing Enhanced Porosity Concrete using electrical impedance to predict acoustic and hydraulic performance, Cement Concr. Res. 36 (2006) 2074–2085.

[45] A. Ibrahim, E. Mahmoud, M. Yamin, V.C. Patibandla, Experimental study on Portland cement pervious concrete mechanical and hydrological properties, Construct. Build. Mater. 50 (2014) 524–529.

[46] R. Fediuk, et al., Acoustic properties of innovative concretes: a review, Materials 14 (2021) 1–28.

[47] T.S. Tie, et al., Sound absorption performance of modified concrete: a review, J. Build. Eng. 30 (2020), 101219.

[48] G. Skjåk-Bræk, H. Grasdalen, O. Smidsrød, Inhomogeneous polysaccharide ionic gels, Carbohydr. Polym. 10 (1989) 31–54.

[49] S.N. Pawar, K.J. Edgar, Alginate derivatization: a review of chemistry, properties and applications, Biomaterials 33 (2012) 3279–3305.

[50] S.K. Bajpai, S. Sharma, Investigation of swelling/degradation behaviour of alginate beads crosslinked with Ca2+ and Ba2+ ions, React. Funct. Polym. 59 (2004) 129–140.

[51] S.K. Motwani, et al., Chitosan-sodium alginate nanoparticles as submicroscopic reservoirs for ocular delivery: formulation, optimisation and in vitro characterisation, Eur. J. Pharm. Biopharm. 68 (2008) 513–525.

[52] G.T. Grant, E.R. Morris, D.A. Rees, P.J.C. Smith, D. Thom, Biological interactions between polysaccharides and divalent cations: the egg-box model, FEBS Lett. 32 (1973) 195–198.

[53] ISO 10534-2:1998, Acoustic – Determination of Sound Absorption Coefficient and Impedance in Impedance Tubes – Part 2: Transfer-Function Method, International Organization for Standardization, Geneva, Switzerland, 1998.

[54] N. Kino, T. Ueno, Investigation of sample size effects in impedance tube measurements, Appl. Acoust. 68 (2007) 1485–1493.

[55] EN 12664:2001. EN 12664:2001, Thermal Performance of Building Materials and Products. Determination of Thermal Resistance by Means of Guarded Hot Plate and Heat Flow Meter Methods - Dry and Moist Products of Medium and Low Thermal Resistance, 2001.

[56] ISO 12570:2000 - Hygrothermal Performance of Building Materials and Products — Determination of Moisture Content by Drying at Elevated Temperature, International Organization for Standardization, Geneva, Switzerland, 2000.

[57] Y. Wang, et al., Accelerators for normal concrete: a critical review on hydration, microstructure and properties of cement-based materials, Cem. Concr. Compos. 134 (2022), 104762.

[58] R. Malheiro, G. Meira, M. Lima, N. Perazzo, Influence of mortar rendering on chloride penetration into concrete structures, Cem. Concr. Compos. 33 (2011) 233–239.

[59] M.F. Montemor, A.M.P. Simões, M.G.S. Ferreira, Chloride-induced corrosion on reinforcing steel: from the fundamentals to the monitoring techniques, Cem. Concr. Compos. 25 (2003) 491–502.

[60] W.S. Yum, et al., Effects of CaCl2 on hydration and properties of lime(CaO)-activated slag/fly ash binder, Cem. Concr. Compos. 84 (2017) 111–123.

[61] M.A. Stumpf González, F. Flach, J. Reschke Pires, M. Piva Kulakowski, Acoustic absorption of mortar composites with waste material, Arch. Acoust. 38 (2013) 417–423.